JOURNAL OF APPLIED ELECTROCHEMISTRY **16** (1986) 517–526

Correlation of electrochemical and ellipsometric data in relation to the kinetics and mechanism of Cu_2O electroformation in alkaline solutions

M. R. GENNERO DE CHIALVO, J. O. ZERBINO, S. L. MARCHIANO, A. J. ARVIA*

Instituto de Investigaciones Fisicoquímicas Teóricas y Aplicadas – INIFTA, Casilla de Correo 16, Sucursal 4, (1900) La Plata, Argentina

Received 7 February 1985; revised 7 July 1985

The kinetics of copper anodization were studied in the potential range of Cu_2O electroformation in different alkaline solutions by using voltammetric, rotating disc electrode, rotating ring–disc electrode and ellipsometric techniques. Thin layer and massive copper electrodes were employed. Results indicate the formation of soluble Cu(I) species at the early stage of copper anodization. Other soluble Cu(II) species are produced after the Cu_2O layer electroformation. Data are discussed on the basis of a reaction mechanism involving different reaction products and the influence of the copper surface on the initial electrochemical reaction.

1. Introduction

The electrochemistry of copper in alkaline solution in the potential range of Cu(I) oxide electroformation and electroreduction is rather complex as these reactions involve the appearance of soluble and insoluble Cu(I) and Cu(II) species simultaneously with the formation and disappearance of the different phases. The relative contribution of each reaction, as determined from voltammetric measurements, depends on the range of anodization potential and on the type of potential programme applied to the electrode [1–14], Furthermore, the voltammetric behaviour of the anodic layer depends to a great extent on its history, probably because of changes of structure due to changes in the degree of hydration and disproportionation reactions involving copper species [5, 15]. Most of the reaction pathways already proposed for explaining the copper anodization reaction postulate the electroadsorption of OH species on copper active sites as the initial stage [5, 8, 13]. This reaction, however, seems to depend significantly on the previous treatment of the electrode surface. The following electro-oxidation stage yielding the copper oxide layer implies complex electrochemical–chemical surface kinetics which under certain conditions can be interpreted through a nucleation and growth mechanism [3].

The present work reports new data related to the different stages of copper electro-oxidation in alkaline solutions by using a thin copper layer electrode to avoid the contribution of the substrate in the electrochemical process. In this case, the existence of soluble copper species during the polarization of copper electrodes is confirmed through *in situ* optical measurements and by applying the rotating disc electrode (RDE) and rotating ring–disc electrode (RRDE) techniques. Data reported in this paper offer a sounder basis for discussing the most probable reaction pathway for the electro-oxidation and the electroreduction reactions related to copper electrodes in alkaline solutions.

2. Experimental details

2.1. *Vitreous carbon–thin Cu(s) electrode in NaOH solutions*

Thin copper layers on vitreous carbon discs

* To whom correspondence should be addressed.

0021–891X/86 $03.00 + .12

(Union Carbide, low density, 0.071 cm^2 apparent area) were prepared by potentiodynamic electroreduction of $Cu(OH)_2$ previously deposited on the substrate. First, the carbon disc surface was polished with emery paper gradually changed from No. 600 to alumina powder (0.3 μm diameter average particle size) and later repeatedly rinsed with triply distilled water.

The preparation of the carbon–thin Cu(s) electrode was carried out in two stages, namely the precipitation of $Cu(OH)_2$ on the carbon substrate and the potentiodynamic electroreduction of $Cu(OH)_2$ to Cu(s). $Cu(OH)_2$ was precipitated on the polished carbon disc by alternate immersions in NaOH (10^{-3} M < c_{NaOH} < 1 M) and $CuSO_4$ (10^{-2} M < c_{CuSO_4} < 1 M) solutions. The immersion time (t) in each solution was varied between 1 and 10 s, and the number of immersions (n) was chosen in the $1 < n < 5$ range. Occasionally, Na_2SO_4 (0.1 M < $c_{Na_2SO_4}$ < 1 M) was added to the $CuSO_4$ solution to determine its influence in the characteristics of the $Cu(OH)_2$ precipitate. The vitreous carbon–$Cu(OH)_2$ electrode was placed into a three-compartment Pyrex glass cell with a large area platinum counter electrode and a Hg–HgO–1 M NaOH reference electrode (E_0/(NHE) = 0.100 V) connected through a Luggin–Haber capillary tip. The vitreous carbon–$Cu(OH)_2$ electrode was then subjected to triangular potential sweeps (TPS) from the potential E_a (−0.05 V < E_a < 0.0 V) to the potential E_c (−1.2 V < E_c < −1.1 V) at the potential sweep rate, v (0.02 V s^{-1} < v < 0.3 V s^{-1}) to electroreduce $Cu(OH)_2$ to copper. This reaction requires several potential scans for its completion, depending on the amount of precipitated $Cu(OH)_2$. The response of the first voltammetric scans related to $Cu(OH)_2$ electroreduction depends considerably on the amount of precipitated $Cu(OH)_2$ and the composition and concentration of the precipitating solution, as well as that of the electrolyte. The electroreduction reaction probably involves soluble species such as either CuO_2^{2-} or CuO_2H^-, their relative contributions depending on the concentration of the alkaline solution [5, 13].

Potentials in the text are corrected for the liquid junction potential and given on the NHE scale. Different NaOH solutions (10^{-2} M < c_{NaOH} < 1 M) were used as electrolyte, runs were made at 25 ± 0.1° C under N_2 atmosphere.

The vitreous carbon–thin Cu(s) electrode was first subjected to repetitive triangular potential sweeps (RTPS) in the potential range of the Cu–Cu(I) redox couple, and then to different combined potential–time programmes according to the purpose of each run.

2.2. *Rotating disc and rotating ring–disc electrode techniques*

The copper RDE was made by axially fitting a copper rod (99.99% purity, 0.4 cm diameter) in a Teflon rod (1.4 cm diameter). The RRDE consisted of a copper disc (99.99% copper, 0.126 cm^2 apparent area) and a gold ring (0.029 cm^2 apparent area), with a collection efficiency of 0.25. A platinum counterelectrode (4 cm^2) and a Hg–HgO–1 M NaOH reference electrode were used.

Runs were performed at 25 ± 0.1° C in NaOH solutions (10^{-2} M < c_{NaOH} < 2 M) previously deaerated by bubbling purified N_2. Alkaline solutions, with the addition of either $NaClO_4$ (0.01 M < c_{NaClO_4} < 0.1 M), Na_2SO_4 (0.01 M < $c_{Na_2SO_4}$ < 0.1 M) and $Na_2B_4O_7$ (0.01 M < $c_{Na_2B_4O_7}$ < 0.1 M), were also employed. RDE and RRDE were used at rotation speeds (ω) ranging from 500 to 7000 r.p.m. Before each run the copper disc was subjected to a RTPS at a preset v ranging from a value of E_c set in the H_2 evolution potential range to a value of E_a in the region of Cu_2O electroformation. Potential cycling was continued until a stable and reproducible voltammogram was obtained. Once this condition was achieved, conventional voltammograms were run at the disc under RTPS at 0.01 V s^{-1} < v < 0.5 V s^{-1} and $0 < \omega < 7000$ r.p.m., and the current at the disc was measured at a preset potential simultaneously.

Another type of potential programme applied to the electrode consisted of a RTPS combined with potential steps at E_s (−0.30 V < E_s < 0.15 V) held during the time (τ) (1 s < τ < 180 s). For the latter, the corresponding current transients at a constant potential, E_R, were also recorded at the ring. The values of E_R (−0.6 V < E_R < 0.05 V) were preset either at the positive or

at the negative side of the equilibrium potential of the Cu–Cu_2O redox couple [13].

2.3. *Ellipsometric measurements*

A copper disc (99.9% purity, 0.50 cm^2 apparent area) working electrode was used in the ellipsometric measurements. Before each run the electrode was polished to a mirror surface with alumina powder (0.05 μm particle size). Runs were made in 0.1 M NaOH at room temperature under N_2. The electrolysis cell was mounted in a Rudolph Research type 437-02/200 B manual ellipsometer (maximum resolution 0.01°) provided with a 24 V–150 W tungsten lamp, a filter (5461 Å) and a RCA/P2/ photomultiplier. The incidence light beam angle was fixed at 71° and the angle of the compensator at 135°.

The refraction index (n_s) and absorption coefficient (k_s) of the substrate were obtained from the polarizer (P) and analyser (A) using a polished copper electrode held at −1.2 V. The resulting values (n_s = 0.802 and k_s = 2.48) are in good agreement with previously reported data [7, 16].

Most reproducible data were obtained by continuously measuring both P and A during a potential sweep at 1.5 mV s^{-1} in both positive and negative potential going directions. Changes in P were also determined through the changes in the intensity of the reflected light [17, 18] during the RTPS at 1.5 mV s^{-1}. The small changes in reflectivity (less than 2%) were produced by changes in the layer thickness.

P_0 and A_0 were taken as reference values for the dynamic measurements, the zero subscript denoting the extinction orientation. Thus for A = 30.1° and P set at $(P - P_0)$ = 31.5 of extinction, the changes in the light intensity with the applied potential depend mainly on P and are practically independent of A.

3. Results

3.1. *Voltammograms run with vitreous carbon–thin Cu(s) electrodes*

The first voltammogram run with a vitreous carbon–thin Cu(s) electrode in 0.1 M NaOH at 0.1 V s^{-1} from E_a = −0.04 V to E_c = −1.18 V (Fig. 1a) shows three cathodic peaks at −0.22 V, −0.45 V and −0.93 V, respectively, which correspond to the electroreduction of Cu(II) and Cu(I) species. The reverse potential scan exhibits an anodic peak at −0.10 V, the charge of the latter (Q_a) increasing during cycling up to a certain limit. In this case the stabilized voltammogram, reached after about 2 min RTPS, shows (Fig. 1b), in addition to the anodic (API) and cathodic (CPI) current peaks already described in previous work [6, 13, 14], a small complex anodic peak at about −0.35 V. This precedes the anodic peak assigned to Cu_2O electroformation at −0.10 V. The voltammogram of the thin copper layer is similar to that for bulk copper, except that the contribution of the anodic pre-peak is considerably enhanced and that the voltammetric charge decreases continuously during cycling (Fig. 1b). It appears that the contribution of the pre-peak tends to disappear faster than that of the main anodic peak. This effect, which had already been observed in other thin electrodeposited metal electrodes [19], can be attributed to sintering of

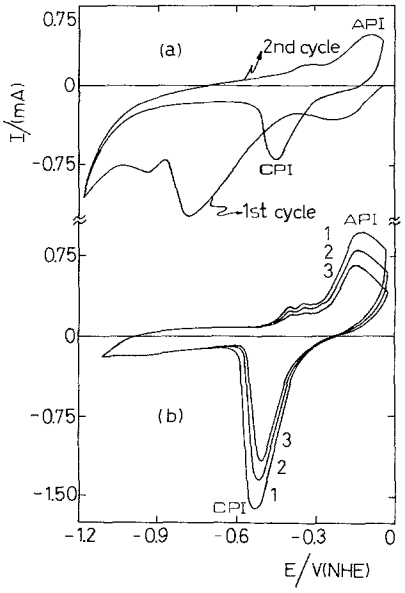

Fig. 1. (a) Voltammograms (first negative going scan for electroreducing the $Cu(OH)_2$ layer and second repetitive triangular potential scan). (b) Voltammograms after applying a repetitive triangular potential scan for different times (t). 1, t = 10 min; 2, t = 20 min; 3, t = 30 min. Vitreous carbon–$Cu(OH)_2$ electrode in 0.1 M NaOH, v = 0.1 V s^{-1}, apparent electrode area 0.071 cm^2, 25° C. Electrode preparation t = 5 s; n = 3 in 0.1 M NaOH and 0.1 M $CuSO_4$.

the copper layer, a process which is probably slower than those involved in the proper electroformation and electroreduction of the Cu_2O layer. Hence, the enhancement of the anodic pre-peak can be related to the properties of the thin copper layer electrode as it occurs for the voltammetric behaviour of other thin metal electrodes [20, 21].

3.2. *Voltammograms run with bulk copper electrodes*

The appearance of the anodic pre-peak when bulk copper electrodes are used is not conclusive [8]. However, the results obtained with thin copper layer electrodes suggest that bulk copper electrodes subjected to a predetermined combined potential perturbation should also provide information regarding the anodic pre-peak. For the purpose, the copper electrode was first subjected to a RPTS at $0.2\,V\,s^{-1}$ to obtain the stabilized voltammogram (Fig. 2, dashed line). Immediately following this, the potential was stepped to 0.02 V for 5 min, that is in the potential range of Cu(II) electroformation (0.20 V), and later stepped to -1.3 V for 5 min, in the H_2 evolution potential range. The conventional voltammogram resulting from this treatment (Fig. 2, full line) shows the complex anodic pre-peak already described in vitreous carbon–thin copper electrodes. In these cases, the appearance of the anodic pre-peak is accompanied by the reversible redox couple at about -0.74 V. The voltammetric charge related to both the anodic pre-peak and the redox couple is relatively small, probably in the order of one monolayer of adsorbed species.

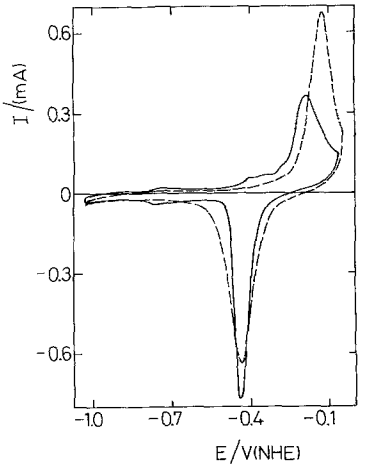

Fig. 2. Voltammograms run with a massive copper electrode. (– – –), stabilized I/E profile; (——), profile resulting after holding the potential at 0.2 V (5 min) and at -1.3 V (5 min) before the negative and the positive potential going scan, respectively. Apparent electrode area $0.322\,cm^2$; 0.1 M NaOH; $v = 0.2\,V\,s^{-1}$; 25° C.

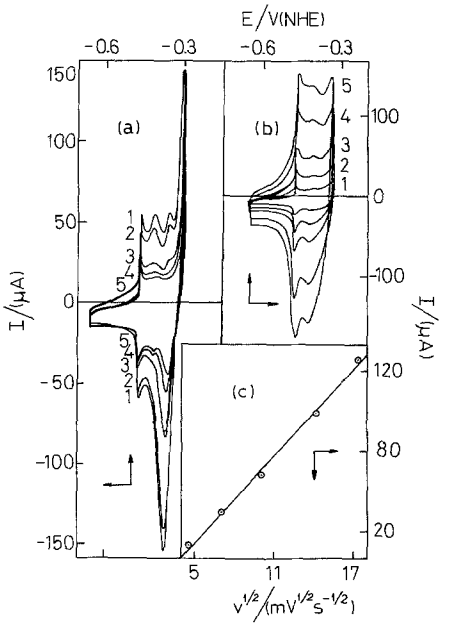

Fig. 3. (a) Voltammograms corresponding to the first (1) and second (2) RTPS and after 10 min (3), 30 min (4) and 40 min (5) RTPS at $0.02\,V\,s^{-1}$. (b) Voltammograms run at different v. 1, $0.02\,V\,s^{-1}$; 2, $0.05\,V\,s^{-1}$; 3, $0.1\,V\,s^{-1}$; 4, $0.2\,V\,s^{-1}$; 5, $0.3\,V\,s^{-1}$. (c) Dependence of the height of API on $v^{1/2}$ in still solution. Massive copper electrode; apparent electrode area $0.322\,cm^2$; 0.1 M NaOH; 25° C.

The voltammogram in the potential range of the anodic pre-peak (Fig. 3a, b) shows, in the first potential scan, at least three different current contributions which during the following scans change to a double pair of conjugated current peaks. The charge of the first pre-peak is nearly independent of v, but the corresponding peak height increases linearly with v (Fig. 3c).

3.3. *Voltammograms run with RDE and RRDE*

The voltammograms run at a constant v and different ω (Fig. 4) show a slight dependence on ω. The height of the main anodic peak (API) (j) increases very slightly with ω, approaching different j versus $\omega^{1/2}$ straight-line relationships,

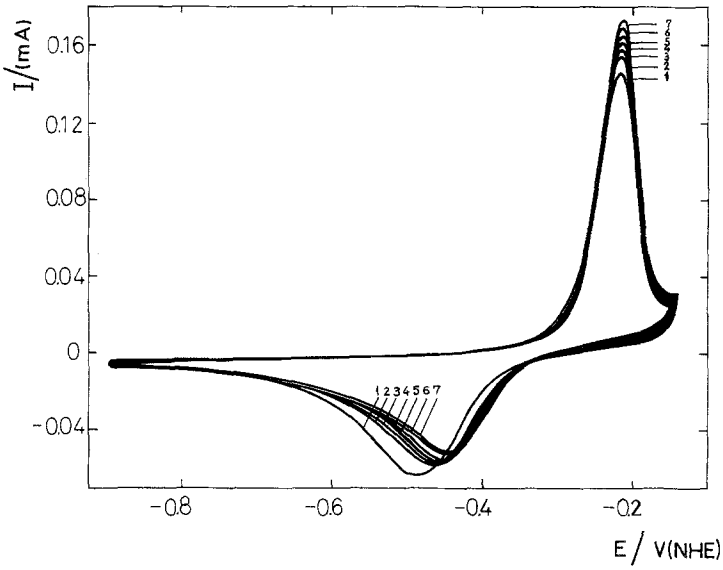

Fig. 4. Influence of ω on the voltammograms obtained with a copper RDE. 1, 0 r.p.m.; 2, 500 r.p.m.; 3, 1000 r.p.m.; 4, 2000 r.p.m.; 5, 3000 r.p.m.; 6, 5000 r.p.m.; 7, 7000 r.p.m. Apparent electrode area 0.125 cm^2, 1 M NaOH, v = 0.05 $V s^{-1}$, 25° C.

according to the NaOH concentration (Fig. 5). These lines do not intercept the origin of the plot and their slopes are much smaller than those expected for a simple convective diffusion process at the RDE. Conversely as ω increases, the height of the cathodic peak, CPI, decreases and its potential becomes more positive.

Runs made either by fixing v and changing ω or vice versa can be correlated by plotting the anodic peak height against $(v/\omega)^{1/2}$. These plots give two sets of curves which can be interpreted in terms of either v or ω being constant, respectively (Fig. 6). At large $(v/\omega)^{1/2}$ values when v changes from 0.01 $V s^{-1}$ to 0.5 $V s^{-1}$ the slopes of those plots obtained with 0.1 M NaOH vary from 0.9 to 0.3, while those of 0.1 M NaOH vary from 0.125 to 0.01.

The electroreduction voltammogram resulting after applying linear potential sweeps combined with a potential step at $E_a = E_D$ (Fig. 7) [13] to a still copper disc electrode shows three peaks (CPI,CPII and CPIII), their relative contributions depending on E_D, v, and NaOH concentration. A particular set of these parameters is associated with the maximal splitting in the

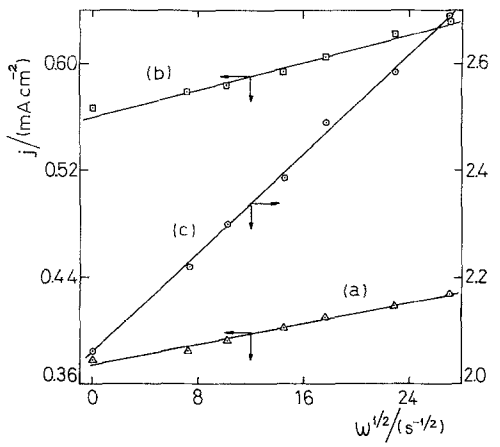

Fig. 5. Dependence of the height of API versus $\omega^{1/2}$. (a) 0.01 M NaOH, (b) 0.1 M NaOH, (c) 1 M NaOH. Electrode characteristics are indicated in Fig. 4, v = 0.05 $V s^{-1}$, 25° C.

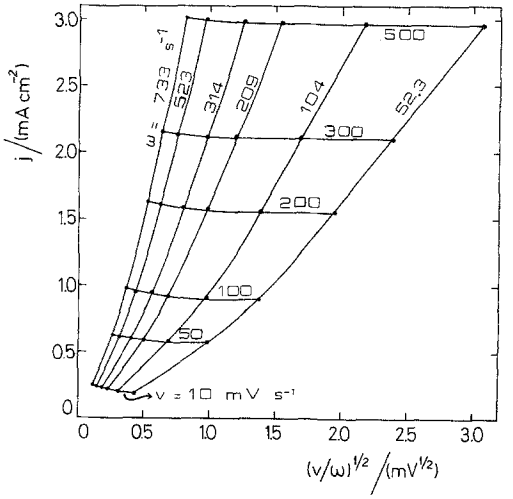

Fig. 6. Dependence of j on $(v/\omega)^{1/2}$. Lines represent v = constant and ω = constant conditions. 0.1 M NaOH, 25° C.

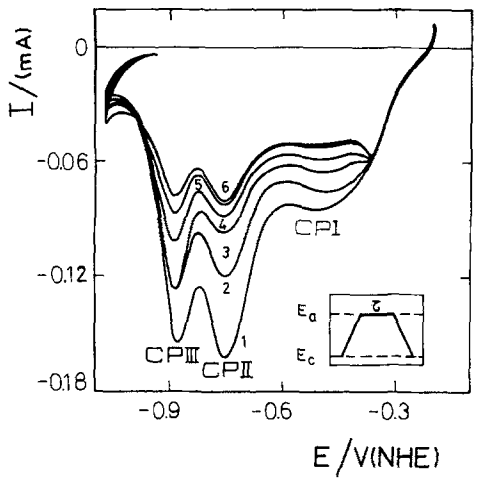

Fig. 7. Electroreduction voltammograms obtained with a copper RDE after applying the perturbation programme depicted in the figure. 1, 0 r.p.m.; 2, 500 r.p.m.; 3, 1000 r.p.m.; 4, 3000 r.p.m.; 5, 5000 r.p.m.; 6, 7000 r.p.m. 0.1 M NaOH, $\tau = 30$ s, $E_a = -0.2$ V, $v = 0.2$ V s^{-1}, apparent electrode area 0.125 cm^2, 25° C.

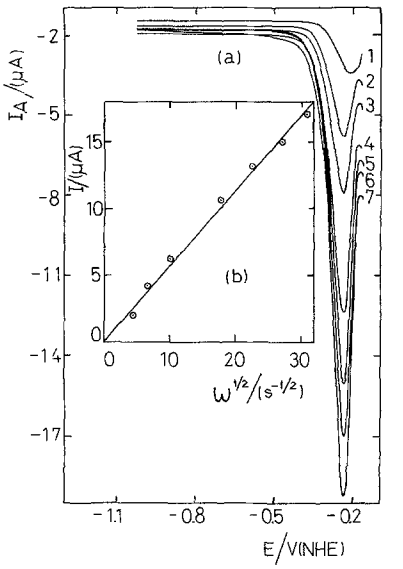

Fig. 8. (a) Ring current versus disc potential profiles obtained with the RRDE. 1, 200 r.p.m.; 2, 500 r.p.m.; 3, 1000 r.p.m.; 4, 3000 r.p.m.; 5, 5000 r.p.m.; 6, 7000 r.p.m.; 7, 9000 r.p.m. (b) Height of the current peak at the ring electrode versus $\omega^{1/2}$. 1 M NaOH, v (disc) = 0.05 V s^{-1}, $E_R = -0.5$ V, apparent electrode area 0.029 cm^2, 25° C.

electroreduction voltammogram [13]. Runs made with rotation show that the cathodic charge decreases with increasing ω before reaching the limiting charge value 1.7 mC cm^{-2} at $\omega = 5000$ r.p.m. The height of CPI appears independent of ω while that of CPII decreases as ω increases. The response of CPI can be related to a surface process, that of CPII should involve the transport controlled dissolution of a surface phase and that of CPIII comprises the electroreduction of soluble Cu(II) species formed during the anodic run.

Runs were made with the RRDE under different perturbation conditions. Thus, when the ring electrode is held at a constant potential (E_R) and the disc electrode is subjected to a RTPS from the H_2 evolution potential range to -0.5 V at 3000 r.p.m., the magnitude and sign of the current at the ring (I_R) depends on E_R (-0.45 V $< E_R < -0.05$ V) [13]. At $E_R = -0.5$ V a cathodic current peak is observed at the ring which increases linearly with $\omega^{1/2}$ (Fig. 8).

Current transients were also measured by holding the ring at E_R and simultaneously the disc electrode at E_D. In this case, E_R ranged from -0.125 V to -0.625 V. The charge collected at the ring electrode (Q_R) depends on E_D (Fig. 9) and goes through a maximum when E_D is in the -0.20 V to -0.25 V range. This potential range coincides with that where the maximum splitting in the electroreduction voltammogram is observed [13].

For $E_R = -0.625$ V a further increase in Q_R is noticed when $E_D = -0.125$ V, due to the formation of Cu(II) soluble species. The latter is electroreduced at the ring electrode simultaneously with the Cu(I) species formerly produced.

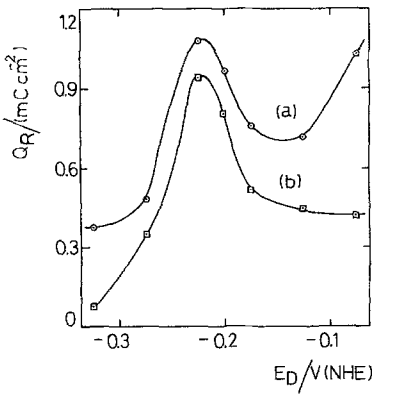

Fig. 9. Charge obtained from current transients at the ring electrode versus E_D. The disc electrode was potential stepped from $E_c = -1.1$ V to E_D. The potential step at E_D was held for $\tau = 30$ s. (a) $E_R = -0.625$ V, (b) $E_R = 0.125$ V. 0.1 M NaOH, 3000 r.p.m., 25° C.

3.4. *Ellipsometric measurements*

Ellipsometric data which are plotted in the Δ versus ψ plane can be directly compared to those computed from the simplest structure of the metal–single oxide layer–solution inferface. The parameters $\Delta\,(=90+2P)$ and $\psi\,(=A)$ are related to the complex refractive index ($n_s = n - ik_s$) and thickness (d) of the oxide layer [18]. The values of P and A for the polished copper electrode are 176.19° and 37.71°, respectively. Calibration was carried out by relating unit lengths of the chart paper to angular positions of the polarizer (29°, 30°, 31° off extinction) [17]. From the plots depicted in Fig. 10 the most likely values of n_s, k_s and d of the oxide layer are obtained. The fitting was made for $n_s = 2.0$, $0.0 < k_s < 0.8$, and $0 < d < 50$ Å [7, 22].

Dynamic ellipsometric measurements at $0.0015\,V\,s^{-1}$ between -1.2 V and 0.07 V, i.e. in the potential range where Cu(I) species are produced, show only a slight variation in ψ but changes of Δ were between 4 and 5°. On the other hand, at the end of the negative potential going scan the values of Δ and ψ nearly reproduce the former values assigned to the bare copper surface ($\delta\Delta_0 = 0.055°$; $\delta\psi_0 = 0.07°$). From these results it may be concluded that in this case the thickness of the overall anodic oxide layer is lower than 50 Å, and after reduction the surface roughness contribution to the change of Δ_0 is less than 2%. Different results are obtained when the potential applied to the electrode is sufficiently positive to produce Cu(II) oxide. In this case a larger change in the values of P_0 and

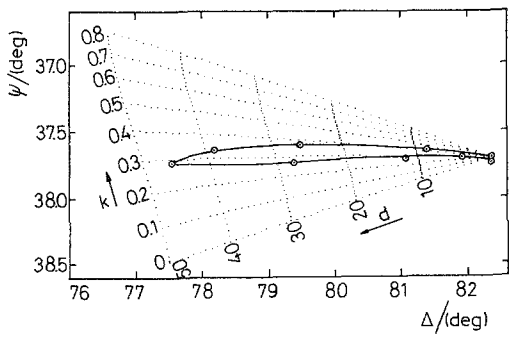

Fig. 10. Plot of Δ versus ψ. (···), Computed data from a single homogeneous layer model ($n = 2.0$); (——), experimental results. 0.1 M NaOH, apparent electrode area $0.50\,cm^2$, $v = 0.0015\,V\,s^{-1}$.

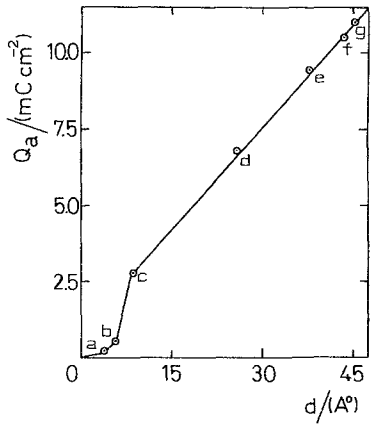

Fig. 11. Anodic charge versus film thickness plot from extinction ellipsometry. 0.1 M NaOH, apparent electrode area $0.50\,cm^2$, $v = 0.0015\,V\,s^{-1}$. Data obtained from the positive potential going scan at (a) -0.27 V; (b) -0.22; (c) -0.17 V; (d) -0.12 V; (e) -0.07 V; (f) -0.12 V; (g) -0.17 V. Letters in Figs 11 and 12 correspond to the same potential values.

A_0 is observed after reduction of the Cu(II) oxide layer.

In the present case no influence of illumination on the voltammetric response of the system was observed. Photo effects have been reported for the oxidation processes of copper electrodes and the reduction of Cu_2O by using intermittent chronoellipsometry and photoelectric techniques [7].

Taking into account that fact that ψ remains almost constant, the changes in Δ can be principally associated with changes in d. In the potential range corresponding to the ascending branch of API (-0.22 V to -0.17 V) the Q_a versus d plot (Fig. 11) shows a considerable increase in Q_a at a nearly constant value of d. Later, there is a linear relationship between Q_a and d. Dynamic measurements of Δ show that the changes in Δ begin when the potential scan reaches the potential of API (Fig. 12). These results are in agreement with those derived from the RRDE and confirm that soluble Cu(I) species are formed in the early stages of Cu_2O electroformation from copper in base electrolyte.

3.5. *Influence of electrolyte composition*

The voltammograms of Cu_2O electroformation

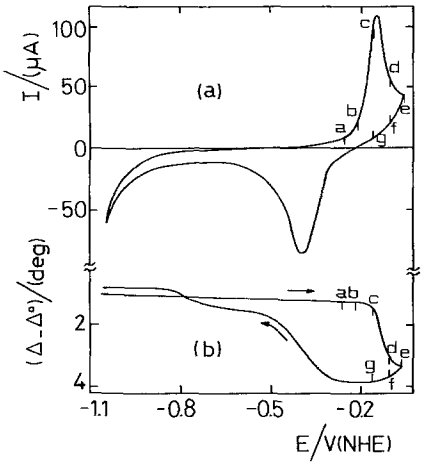

Fig. 12. Correlation between the voltammetric and the dynamic ellipsometric responses. (a) Voltammogram of a copper electrode and (b) simmultaneous change of $(\Delta - \Delta_0)$–potential profile. Apparent electrode area 0.50 cm^2, 0.1 M NaOH, $v = 0.0015\,V\,s^{-1}$.

and electroreduction in different alkaline electrolytes show no substantial qualitative changes due to the electrolyte composition, except that in NaOH + $Na_2B_4O_7$ solutions the currents related to API are lower than those recorded in either plain NaOH solutions or in NaOH + $NaClO_4$ solutions. The addition of Na_2SO_4, however, produces the reverse effect (Fig. 13). The dependence of the height of API on the rate of stirring also changes with the composition of the electrolyte solution. At a constant ionic strength the slopes of the API height versus $\omega^{1/2}$

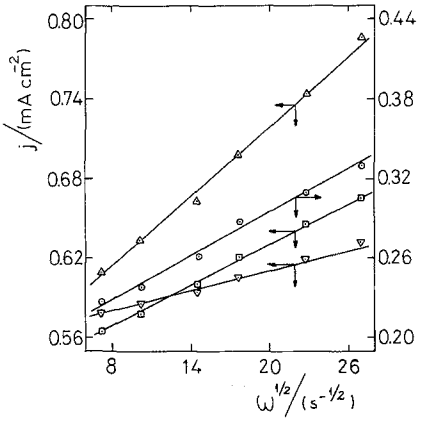

Fig. 13. Dependence of the height of API on $\omega^{1/2}$ for different solution compositions. ▽, 0.1 M NaOH; □, 0.1 M NaOH + 0.05 M $NaClO_4$; △, 0.1 M NaOH + 0.05 M Na_2SO_4; ○, 0.1 M NaOH + 0.05 M $Na_2B_4O_7$. Apparent electrode area 0.125 cm^2, $v = 0.05\,V\,s^{-1}$, 25° C.

linear plots increase in the order NaOH < $Na_2B_4O_7 \simeq NaClO_4 < Na_2SO_4$.

4. Discussion

The voltammetric response of thin copper electrodes in stagnant solution, the voltammetric data with stirring and the ellipsometric results obtained in the Cu_2O potential range suggest three main processes in the anodization of copper in alkaline solutions. These are the initial reaction which is the underpotential decomposition of water yielding adsorbed OH species in the order of one monolayer thickness, the electrodissolution of copper producing soluble species, and the growth of the Cu_2O layer.

4.1. *Precursor layer and dynamic aspects of the copper surface*

The precursor layer of adsorbed OH is related to both the anodic pre-peaks shown in Fig. 1 and the initial portion of the Q_a versus d plot (Fig. 11). According to the latter, the average thickness of the precursor layer should be less than 5 Å, in agreement with previous results [8]. The structure of the precursor layer can be regarded as a $Cu(OH)_{ad}$ species (Fig. 14, reactions Ia and Ib) involving at least two types of reactive centres, copper* and copper. The relative contribution of reaction Ia to reaction Ib increases in freshly formed thin electrode surfaces (Figs 1, 2). The copper surface under a transient perturbation behaves as a dynamic system as the copper* species, being the most reactive, stabilizes to the copper species (Fig. 14, reaction Ic). This type of process, already reported for non-stationary electrochemical responses of different metals, is associated with surface reconstruction, faceting and sintering [19]. The stabilization of copper* to copper can also occur, in principle, through species such as Cu*(OH) or Cu_2^*O (reactions Id and IIc in Fig. 14). These possibilities are not conclusively derived from the voltammetric data although they are inferred from the ageing effect of the anodic layer previously reported [5, 6].

On the other hand, the copper*–copper surface concentration ratio is apparently greater as the electrode roughness increases. In this case

the electrode roughness can be estimated through the voltammetric charge involved in the double layer region. Roughness effects are accomplished in different ways, namely by using thin copper electrodes on carbon and by extending E_a to sufficiently positive values so that Cu(II) soluble species are formed and later electroreduced during the negative going potential scan. In principle the correlation between roughness and magnitude of anodic charge corresponding to the anodic pre-peak can be explained in terms of grain size distribution at the surface which increases the copper*–copper surface concentration ratio. In this case the copper* centres might be related to atoms at the grain borders and copper centres to atoms at the grain surfaces. Hence, the distribution of active centres might be most important in determining the enhancement of the electrochemical reactivity of copper [14].

4.2. *Formation of soluble species*

The electrodissolution of copper yielding Cu(I) soluble species is already observed before the electroformation of bulk Cu_2O takes place. Soluble Cu(I) in the alkaline solution has been related to the formation of ionic species such as $Cu_2O_2H^-$ or $Cu_2O_2^{2-}$ [13] either from $Cu(OH)_{ad}$ or Cu_2O (Fig. 14, reactions IIIa and IIIb). The two soluble species participate in equilibrium (Fig. 14, reaction IIIc) which depends on the pH of the solution. Furthermore, soluble Cu(I), in part, undergoes a disproportionation reaction into soluble Cu(II) and Cu(s) (Fig. 14, reaction IVa). Certainly, the greatest yield of soluble Cu(II) species results from further electro-oxidation of the various Cu(I) species.

Ellipsometric and RRDE data demonstrate that the largest contribution of soluble species corresponds to the early stage of anodization. It should be noted that the voltammetric responses, related to the existence of the various soluble copper species indicated in the reaction mechanism, are suppressed in the presence of precipitating ions in solution, such as sulphide ion [15]. This gives further support to the reaction mechanism presented in Fig. 14.

4.3. *Formation and growth of the Cu_2O layer*

The formation and growth of the hydrous Cu_2O layer is explained in terms of reactions IIa and IIb (Fig. 14). The oxide layer also participates in a dissolution process as indicated by reaction IIIb. As the charge at the ring electrode goes through a maximum for $-0.25\,V < E_D < -0.20\,V$ (Fig. 9) just in the potential range

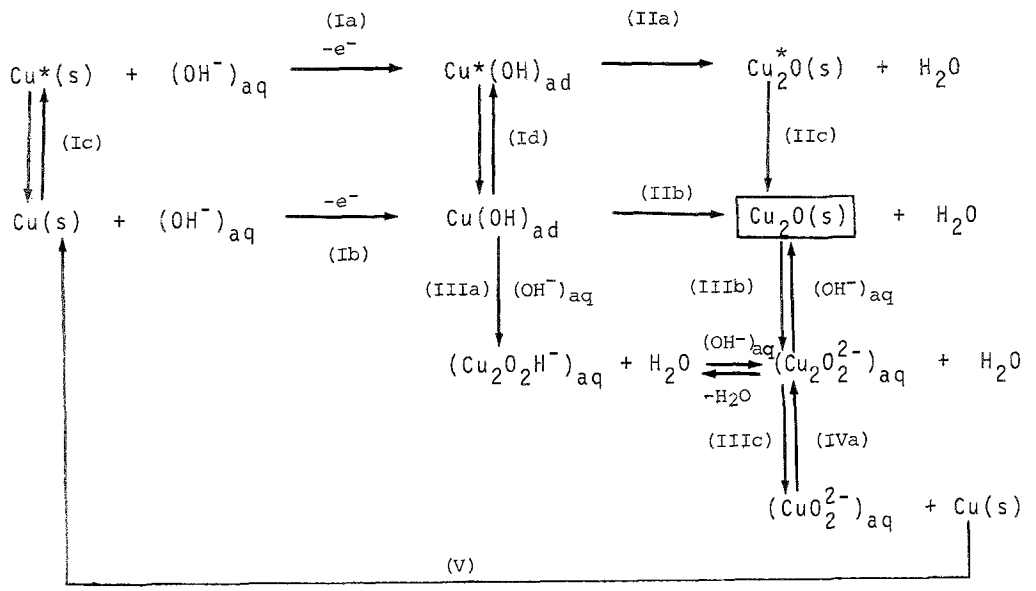

Fig. 14. Reaction pathway (electro-oxidation reaction).

corresponding to peak API, the maximum rate of formation of Cu_2O should be related to the maximum rate of formation of soluble copper species. These results, which are consistent with the maximum contribution of peak PCII and PCIII related to the electroreduction of soluble species, suggest that Cu_2O phase formation occurs, at least in part, through a dissolution and precipitation mechanism. This process is the sum of reactions Ia, Ib, IIIa, IIIb and IIIc in Fig. 14. Furthermore the formation of Cu(s) through reaction IVa also contributes to the growth of the Cu_2O(s) as indicated by the arrow (V) in Fig. 14. Therefore, the overall hydrous Cu_2O layer growth can be presented as the sum of phase formation, electrochemical dissolution reactions and a further chemical precipitation of Cu_2O.

The reaction mechanism depicted in Fig. 14 to explain the voltammetric growth of the hydrous Cu_2O layer in base solution is apparently valid for different electrolyte compositions. The influence of the latter on the height of current peak API can be considered in two ways, namely by competing with the electroadsorption of OH species in the early stages of the reaction as it occurs in the oxygen-electroadsorption on noble metals [23], and by changing the resistance of the hydrous Cu_2O layer through the different solvation of ions inserted into the oxide layer. This second possibility accounts for the electrochemical and ellipsometric behaviour of transition metal hydroxide electrodes in different electrolytes at a constant pH [26, 27].

Acknowledgements

INIFTA is a Research Institute jointly established by the Universidad Nacional de La Plata, the Consejo Nacional de Investigaciones Científicas y Técnicas and the Comisión de Investigaciones Científicas de la Provincia de Buenos Aires. MRGC belongs to the research staff of PRELINE (Programa de Electroquímica Aplicada e Ingeniería Electroquímica).

References

[1] B. Miller, *J. Electrochem. Soc.* **116** (1969) 1675.
[2] J. Ambrose, R. G. Barradas and D. W. Shoesmith, *J. Electroanal. Chem.* **47** (1973) 47, 65.
[3] D. W. Shoesmith, T. E. Rummery, D. Owen and W. Lee, *J. Electrochem. Soc.* **123** (1976) 790.
[4] V. Ashworth and D. Fairhurst, *ibid.* **124** (1977) 506.
[5] A. M. Castro Luna de Medina, S. L. Marchiano and A. J. Arvia, *J. Appl. Electrochem* **8** (1978) 121.
[6] S. L. Marchiano, C. I. Elsner and A. J. Arvia, *ibid.* **10** (1980) 365.
[7] M. Yamashita, K. Omura and D. Hirayama, *Surf. Sci.* **96** (1980) 443.
[8] J. M. M. Droog, C. A. Alderliesten, P. T. Alderliesten and G. A. Bootsma, *J. Electroanal. Chem.* **111** (1980) 61.
[9] S. M. Abd El-Haleem and B. G. Ateya, *ibid.* **117** (1981) 309.
[10] D. W. Shoesmith, S. Sunder, M. G. Bailey, G. J. Wallace and F. W. Stanchell, *J. Electroanal. Chem.* **143** (1983) 153.
[11] M. Maja and P. Spinelli, *Gazz. Chim. Ital.* **113** (1983) 347.
[12] F. Centellas, J. A. Garrido, A. Girones, E. Perez and J. Virgili, *Anal. Quím.* **80** (1984) 193.
[13] M. R. Gennero de Chialvo, S. L. Marchiano and A. J. Arvia, *J. Appl. Electrochem.* **14** (1984) 165.
[14] M. E. Martins and A. J. Arvia, *J. Electroanal. Chem.* **165** (1984) 135.
[15] M. R. Gennero de Chialvo and A. J. Arvia, *J. Appl. Electrochem.* **15** (1985) 685.
[16] L. J. Hawekamp, W. Lisowski and G. A. Bootsma, *ibid.* **118** (1982) 1.
[17] V. Brusic, M. A. Genshaw and B. D. Cahan, *Appl. Opt.* **9** (1970) 1634.
[18] B. D. Cahan, J. Horkans and E. Yeager, *Surf. Sci.* **37** (1973) 559.
[19] A. C. Chialvo, W. E. Triaca and A. J. Arvia, *Anal. Asoc. Quím. Arg.* **73** (1985) 23.
[20] R. Tucceri and D. Posadas, *J. Electrochem. Soc.* **128** (1981) 1478.
[21] *Idem, ibid.* **130** (1983) 104.
[22] N. Novak. A. K. Reddy and H. Wroblowa, *J. Electrochem. Soc.* **117** (1070) 733.
[23] M. I. Florit, M. E. Martins and A. J. Arvia, *J. Electroanal. Chem.* **126** (1981) 255.
[24] *Idem, Anal. Asoc. Quím. Arg.* **71** (1983) 361.
[25] *Idem, ibid.* **72** (1984) 71.
[26] R. E. Carbonio, V. A. Macagno and A. J. Arvia, *J. Electroanal. Chem.* **177** (1984) 217.
[27] O. Albani, J. O. Zerbino, J. R. Vilche and A. J. Arvia, *Electrochim. Acta*, in press.